Materials Today Energy 18 (2020) 100564

Contents lists available at ScienceDirect

Materials Today Energy

journal homepage: www.journals.elsevier.com/materials-today-energy/

Crystalline state transformation strategy for improving the catalytic performance of oxygen evolution reaction at high current density

Y. Xu [a], M.A. Khan [a], Z. Chen [a], C. Chen [a], L. Zhang [a, b], D. Ye [a, *], K. Zhao [a], H. Zhao [a, **], X.A. Sun [c], J. Zhang [a]

[a] College of Sciences & Institute for Sustainable Energy, Shanghai University, Shanghai, 200444, PR China
[b] National Research Council Canada, BC, V6T 1W5, Canada
[c] University of Western Ontario, London, N6A 5B8, Canada

ARTICLE INFO

Article history:
Received 9 July 2020
Received in revised form
10 October 2020
Accepted 12 October 2020
Available online 18 October 2020

Keywords:
Solvent substitution strategy
Amorphous phase
Iron-naphthalenedicarboxylic acid
High-performance catalysts

ABSTRACT

Because the oxygen evolution reaction (OER) greatly limits the large-scale application of electrolyzed water, it is crucial to develop and synthesize effective electrocatalysts. Herein, we report a solvent substitution strategy to prepare the iron-naphthalenedicarboxylic acid (Fe-NDC) coordination complex. Through the crystalline state transformation of Fe-NDC from the crystalline to the amorphous phase, the catalytic performance of the prepared catalyst for OER at high current density can be significantly improved under alkaline conditions. Profiting from exposed metal active sites and expanded electron transport channels, amorphous-phase Fe-NDC (AP-Fe-NDC) exhibits stable electrocatalytic activity, with 225 and 333 mV overpotentials at 10 and 500 mA/cm^2, respectively. Moreover, AP-Fe-NDC displays high oxygen yield and faraday efficiency. This rapid and facile strategy will be of immediate benefit to guide the preparation of other high-performance and low-cost OER catalysts.

1. Introduction

The continuous consumption of fossil fuels has caused environmental pollution and energy shortage, promoting the development of renewable energy technologies, such as the metal-air battery, fuel cell, and hydropower, is extremely urgent [1–3]. Electrocatalytic water decomposition is considered a promising method to obtain clean hydrogen energy. However, the rate-determining steps controlled by the O–H cleavage and the O–O formation significantly affect the kinetics of the oxygen evolution reaction (OER), which is a multistep four-electron transfer reaction process [4]. The development of heterogeneous and homogeneous electrocatalysts promises to accelerate OER dynamics and reduce overpotential. Typically, the precious metal (Ru, Ir, and Pt)–based electrocatalysts show high OER catalytic activity. However, their wide application is limited by their high cost, richness in earth abundance, and low inactivation elasticity [5]. Therefore, there is an intense desire to develop electrocatalysts based on transition metals to achieve low overpotential and efficient OER performance [6].

To obtain stable and efficient catalysts, it is necessary to find a robust ligand system that can firmly fix the metal center and such that auto-oxidation does not occur in the oxidizing environment [7]. Coordination polymers with a designable and predictable structure have recently received much attention. However, their negative electrical conductivity and inferior structural stability severely restrict their practical applications [8–10]. Cheng et al. [11] demonstrated that binding of a naphthalenedicarboxylic acid (NDC) ligand to a metal could induce lattice strain, enabling a powerful bifunctional oxygen reduction reaction and OER. Xue et al. [12] suggested that the electronic structure of coordination polymers can be tuned by introducing missing linkers of carboxyferrocene, which improves OER performance of the catalyst. The complex materials have inherent molecular metal centers and can be used as potential active sites for electrocatalysis [13]. The coordinated unsaturated metal center formed in the process of complex catalysis can act as a typical Lewis acid center to accept electrons from the reactant, thereby promoting the related conversion [14]. Using complexes directly as electrocatalysts can provide a large number of molecular metal active sites [15,16].

* Corresponding author.
** Corresponding author.
E-mail addresses: daixinye@shu.edu.cn (D. Ye), hongbinzhao@shu.edu.cn (H. Zhao).

https://doi.org/10.1016/j.mtener.2020.100564
2468-6069/

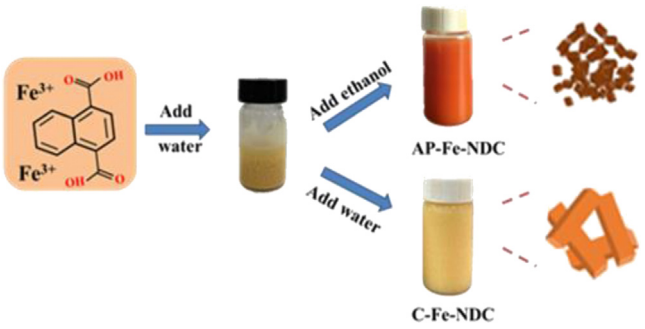

Scheme 1. Illustration of the synthetic process of Fe-NDC. Fe-NDC, iron-naphthalenedicarboxylic acid; AP-Fe-NDC, amorphous-phase iron-naphthalenedicarboxylic acid; C-Fe-NDC, crystalline-phase iron-naphthalenedicarboxylic acid.

Hence, we reported a simple and convenient solvent substitution method to design the iron-NDC (Fe-NDC) complex (see Scheme 1). The complexes were synthesized using ferric nitrate and 1,4-NDC as an organic ligand in a different solvent. Surprisingly, the complex with amorphous phase manifests high catalytic activity for OER, with a low overpotential of 225 mV at the low current density of 10 mA cm^{-2} and 333 mV at the high current density of 500 mA cm^{-2}, with a low Tafel slope for amorphous-phase Fe-NDC (AP-Fe-NDC). Moreover, the characteristics of the low-cost and efficient non-precious catalysts display bright prospects to replace exorbitant noble metal catalysts in industry applications.

2. Results and discussion

To understand the structural characteristics of the synthesized AP-Fe-NDC, the X-ray diffraction (XRD) patterns are shown in Fig. 1a, which is in good agreement with the simulated standard XRD pattern of Fe-NDC, indicating the successful formation of the Fe-NDC complex. Interestingly, the crystallinity degree obtained from the solvent water is high (i.e., crystalline-phase Fe-NDC [C-Fe-NDC]), whereas the crystallinity degree is obviously decreased after immersing into ethanol for several hours. Only one enclosing diffraction peak around at 8.5°, confirming that an AP-Fe-NDC could be formed from crystalline phase and more defects of AP-Fe-NDC might improve the dynamic performance of electrocatalysis. The C-Fe-NDC structure is a six-coordinate octahedral structure (Fig. S1). The Fe ion is surrounded by four O atoms from two different 1,4-NDC ligands and two bridged μ-O atoms from two water molecules [17]. When soaked in the ethanol-water solution, the hydrogen bond interaction between water and NDC is stronger than that between ethanol and NDC [18]. Therefore, as ethanol concentration increases, the interaction between solvent molecules and NDC molecules decreases, resulting in crystal reconstruction, more defects, and smaller particle size. This also has been proved by changing the polarity, miscibility, and wettability of the solvent, the water molecules can be removed to cause the rearrangement of the crystal structure [19]. The electron paramagnetic resonance test further proved that the AP-Fe-NDC complex is rich in defects (Fig. 1b). Such a defect-rich structure indicated the improved performance in the oxygen evolution process.

The thermogravimetric measurements for samples were tested under an air atmosphere (Fig. S2). Clearly distinguishable are the three regions where severe weight losses occur. The first stage loss in mass of Fe-NDC is observed in the range of 30–260 °C with 5–9% weight loss, and it reflects the decomposition of water molecules coordinated by the central metal ion and the release of free water molecules. The second stage observed substantial weight loss in the range of 260–360 °C, and this is due to the structural collapse of the Fe-NDC complex as the ligand was decomposed. The dramatic mass reduction caused by the continuous decomposition of the framework started at 360 °C. The third stage of degradation ends up to 420 °C, which also indicates that Fe-NDC is completely decomposed [20]. In addition, the coordination environment between the Fe^{3+} ion and the ligand was detected via Fourier-transform infrared spectroscopy. As displayed in Fig. 1c, the strong absorption peak near 1679 cm^{-1} was indexed to be the C=O tensile vibration in NDC. The peaks observed at 1562 and 1404 cm^{-1} are identified as asymmetric and symmetric vibrations of the carboxyl group, respectively. The adsorption peak at 779 cm^{-1} is attributed to the vibration of the C–H bond in the benzene ring. In addition, the peak at 475 cm^{-1} is related to the Fe–O tensile vibration [21,22]. The results indicated that the structure is formed by Fe^{3+} and NDC organic ligands. The –COOH can improve the availability of water adsorption on the Fe-NDC inner surface, which accelerates the OER dynamic process.

The surface chemistry is studied via X-ray photoelectron spectroscopy (XPS). The existence of Fe, C, and O elements was confirmed by the XPS spectrum, which is in accordance with the energy-dispersive X-ray spectroscopy (EDS) analysis (Fig. S3). As

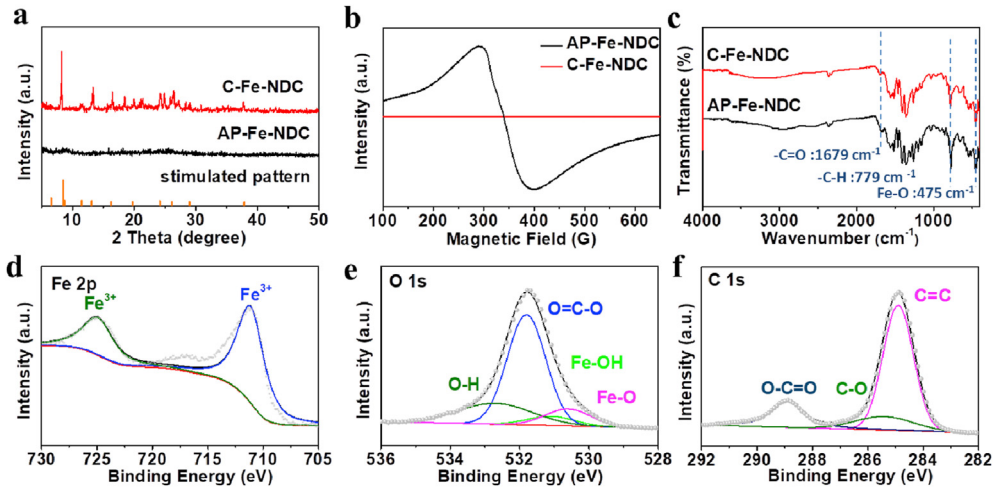

Fig. 1. (a) XRD patterns, (b) EPR spectra and (c) FT-IR spectra of Fe-NDC, and (d–f) XPS of AP-Fe-NDC. XRD, X-ray diffraction; Fe-NDC, iron-naphthalenedicarboxylic acid; AP-Fe-NDC, amorphous-phase iron-naphthalenedicarboxylic acid; C-Fe-NDC, crystalline-phase iron-naphthalenedicarboxylic acid; XPS, X-ray photoelectron spectroscopy; EPR, electron paramagnetic resonance; FTIR, fourier transform infrared.

revealed in Fig. 1d, the peak position of about 711.3 eV (Fe $2p_{3/2}$) and 725.1 eV (Fe $2p_{1/2}$) is attributed to the oxidation state of Fe^{3+} [23]. In the C 1s spectrum, the three peak positions are 284.9 eV, 285.4 eV, and 288.9 eV, which are attributed to the naphthalene ring of NDC, the C—O, and the O—C=O, respectively [7]. As for the O 1s diagram, the absorbed water molecule peak is at 532.7 eV, the —COOH binding peak position of NDC is at 531.8 eV, and the Fe—OH peak is at 531.1 eV [2]. The Fe—O bond is indexed at 530.5 eV, with the content of 39%. The Fe—O bond has been considered to provide an active site for OER [3,4].

The morphology of Fe-NDC was further studied by scanning electron microscopy (Fig. 2a) and high-resolution transmission electron microscopy (HRTEM). The C-Fe-NDC exhibits uniform nanorod-like morphology with a diameter of around 400 nm. But it becomes small nanoparticles after treating with alcohol, confirming that the solvent ethanol evidently changed the NDC structure from the crystalline to amorphous state (Fig. 2b). A larger specific surface area with a small particle size of Fe-NDC is beneficial to the dynamic performance of OER. High-angle annular dark-field-EDS mapping confirmed the good dispersion of Fe, C, and O in AP-Fe-NDC (Fig. S3). The HRTEM image (Fig. 2c) of C-Fe-NDC demonstrates uniform lattice fringes with a spacing of 0.32 nm, which corresponds to the (024) crystal plane. The corresponding fast Fourier Transform represents a monoclinic system. However, no obvious lattice fringes can be seen in the AP-Fe-NDC image (Fig. 2d). The contrast between the two is further verified by selecting area electron diffraction patterns (Fig. S4).

Different from most of the studies on complex electrocatalysts, here, the OER catalytic activity of the obtained AP-Fe-NDC was evaluated without the postcalcination process. A conventional three-electrode system in 1 M KOH was used to explore the OER properties of AP-Fe-NDC. Before performing the catalytic measurements, a preactivation was performed by repeating the CV scan in the potential range of 1.0—1.5 V (vs. RHE) of 50 mV s^{-1} until a steady-state cyclic voltammetry (CV) curve was obtained [1,10,24]. Fig. 3a represents the linear sweep voltammetry curves of different catalysts. For comparison, different ratios of iron and NDC ligands were explored, and the optimal ratio of Fe_1NDC_3 was selected for further investigation (Fig. S5). At a current density of 10 mA cm^{-2}, the overpotential of AP-Fe-NDC, C-Fe-NDC, nickel foam, and IrO_2 is 225 mV, 294 mV, 325 mV, and 236 mV, respectively. This result demonstrates that the amorphous state delivered improved electrochemical performance compared with the crystalline state in the catalytic activity of OER under alkaline conditions. In addition, the AP-Fe-NDC exhibits the sharpest increasing anodic current response for OER, requiring the lowest overpotential to achieve high current densities. From the aforementioned information, AP-Fe-NDC has better OER activity with weak polarization and is superior to the state-of-the-art commercial catalyst IrO_2.

The overpotential at a large current density which could be commercially applied (>500 mA cm^{-2}) was also determined. The obtained AP-Fe-NDC represents excellent performance even at high current densities (the overpotential being only 333 mV at 500 mA cm^{-2}), which is beneficial for practical applications. The catalytic kinetic characteristics of the electrodes, commonly quantified by Tafel slopes, were also investigated and presented in Fig. 3b. The AP-Fe-NDC reveals the lowest Tafel slope (42 mV dec^{-1}), demonstrating substantially rapid reaction kinetics, which should be attributed to the AP-Fe-NDC with small particle size, high wettability, short ion-transfer channel, and a high conjugate structure of AP-Fe-NDC. Moreover, all electrochemical impedance spectroscopy (EIS) spectra are equipped with an equivalent circuit model, which consists of a parallel combination of resistance (R_s) and resistance (R_{ct}) and double-layer capacitance central processing element (CPE). Notably, the R_{ct} of AP-Fe-NDC (1.83 Ω) is significantly lower than that of C-Fe-NDC (2.72 Ω), IrO_2 (2.06 Ω), and nickel foam (NF) (2.2 Ω), as shown in Fig. S6. AP-Fe-NDC manifested the smallest semicircular diameter, elucidating the highest conductivity and fastest catalytic kinetics. Both the

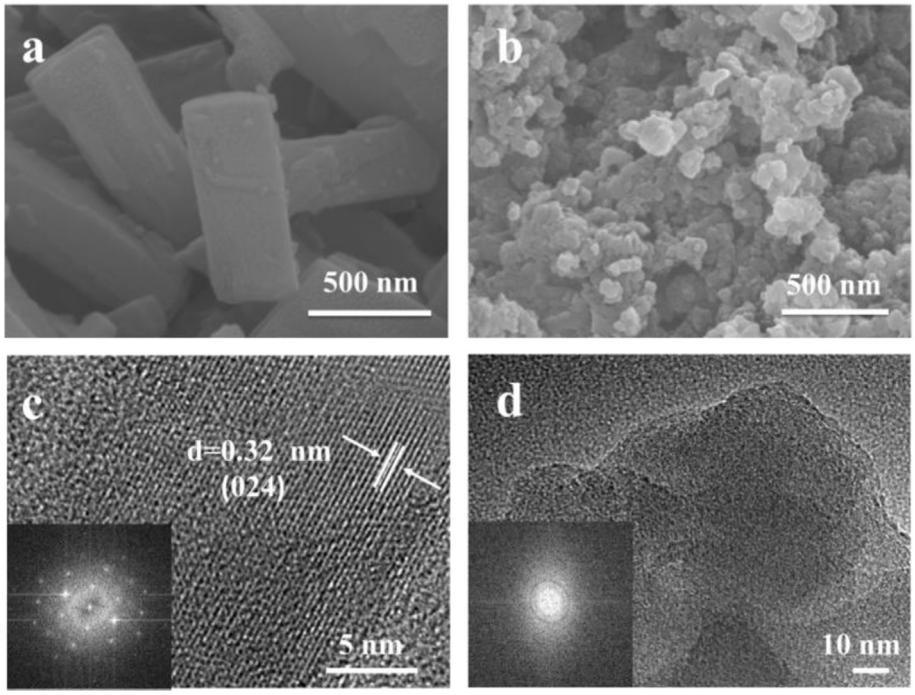

Fig. 2. SEM images of (a) C-Fe-NDC and (b) AP-Fe-NDC; HRTEM images and the corresponding FFT patterns (insets) of (c) C-Fe-NDC and (d) AP-Fe-NDC. SEM, scanning electron microscopy; HRTEM, high-resolution transmission electron microscopy; AP-Fe-NDC, amorphous-phase iron-naphthalenedicarboxylic acid; C-Fe-NDC, crystalline-phase iron-naphthalenedicarboxylic acid; FFT, fast fourier transform.

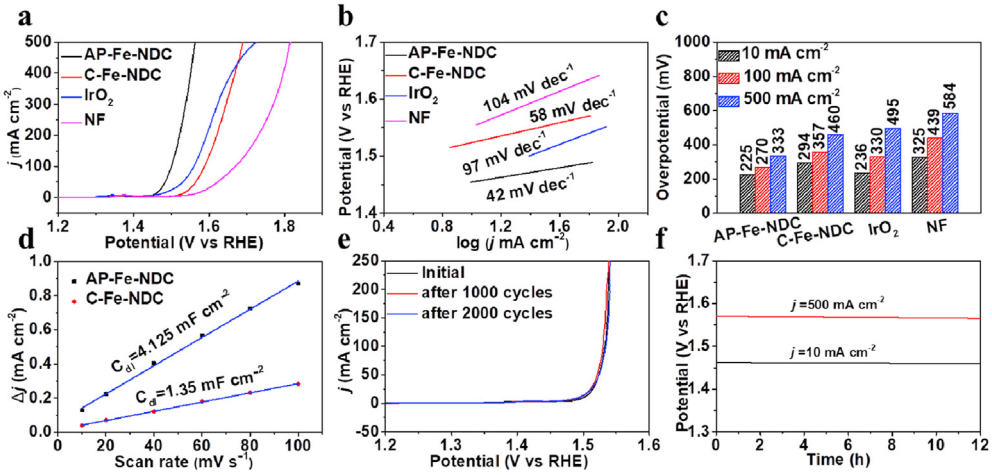

Fig. 3. (a) LSV polarization curves for the OER, (b) corresponding Tafel plots, (c) overpotential to reach the current density of 10 mA cm^{-2}, 100 mA cm^{-2}, and 500 mA cm^{-2}, (d) C_{dl} plots, (e) LSV curves for the OER after different cycles, (f) long-term stability of AP-Fe-NDC. OER, oxygen evolution reaction; C-Fe-NDC, crystalline-phase iron-naphthalenedicarboxylic acid; AP-Fe-NDC, amorphous-phase iron-naphthalenedicarboxylic acid; LSV, linear sweep voltammetry; NF, nickel foam.

crystalline and amorphous complexes have a smaller semicircle diameter than that of IrO_2, which indicates that the prepared catalyst has inherent high electrical conductivity and enhances its OER catalytic activity. This is consistent with its low overpotential and Tafel slope. Fig. 3c visually displays the comparison results of the overpotentials of the four catalysts at different current densities, and further comparison with the published work is shown in Table S1. The results demonstrate the fabulous outperformance of AP-Fe-NDC at both high and low current densities. In addition, the electrochemically active surface areas (ECSAs) of different catalysts were calculated by the double-layer capacitance (C_{dl}), as shown in Fig. 3d. The C_{dl} values of AP-Fe-NDC and C-Fe-NDC are 4.1 and 1.35 mF cm^{-2}, respectively. A higher ECSA value of AP-Fe-NDC suggests more active sites exposed.

The electrochemical stability is another key factor to evaluate the catalytic performance. Fig. 3e and f suggest the outstanding long-term stability of AP-Fe-NDC. The linear sweep voltammetry (LSV) curves well overlapped with that after 2000 cycles. The catalyst sustained for 12 h at both low (10 mA cm^{-2}) and high (500 mA cm^{-2}) current densities, and no obvious attenuation of activity was observed. Furthermore, after a long-term stability test, the XPS results are further analyzed to investigate the changes of AP-Fe-NDC after OER cycling. The spectrum of Fe 2p (Fig. 4a) clearly reflects that the peaks are shifted to higher binding energy (Fe $2p_{3/2}$ at 711.8 eV and Fe $2p_{1/2}$ at 725.4 eV) after 12 h than pristine AP-Fe-NDC (Fe $2p_{3/2}$ at 711.3 eV, Fe $2p_{1/2}$ at 725.1 eV).

This could be ascribed to the structural evolution that occurred during the OER [25].

The electronic structure change of O is also investigated (Fig. 4b), wherein the stronger peaks of O 1s originated from O—H (533.4 eV), Fe—OH (531.1 eV), and Fe—O (530.5 eV), further demonstrating the possible formation of FeOOH [3]. The XPS spectra indicate that the AP-Fe-NDC underwent a transformation into a highly active (oxy)hydroxide phase during the water oxidation process. As the organic ligands are often labile during the electrochemical transformation, the coordinatively unsaturated metal centers would be generated [26], which can accept electrons from the reactants and form the new stable Fe—*O*—OH active sites [16,27]. It can be seen from the XRD results (Fig. S7) that AP-Fe-NDC is converted into FeOOH after the reaction. Hence, the in situ generated FeOOH provides active centers and promotes the enhancement of oxygen evolution. The inductive coupled plasma

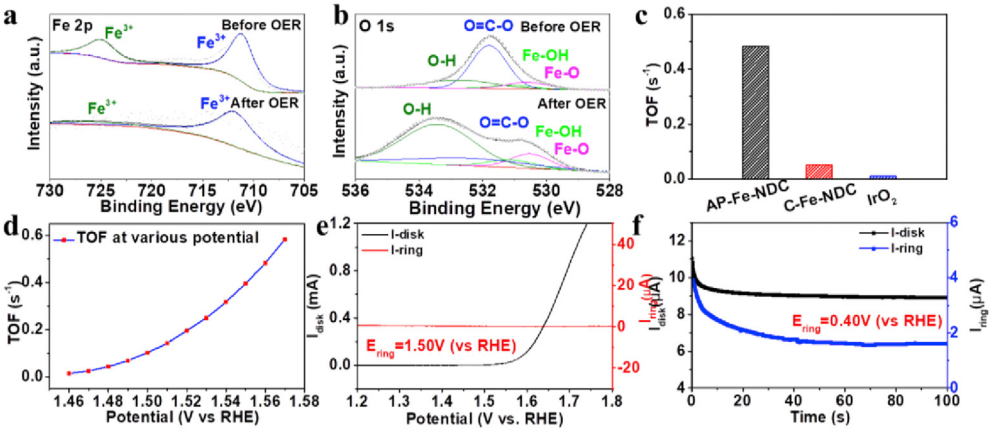

Fig. 4. (a—b) XPS analysis of AP-Fe-NDC before and after the chronoamperometric measurement, (c) TOF values at 330 mV, (d) the TOF plot of AP-Fe-NDC at various potentials, (e) disk and ring current of AP-Fe-NDC tested using the RRDE in 1 M KOH solution, (f) disk and ring current of AP-Fe-NDC tested using the RRDE in N_2-saturated 1 M KOH solution. XPS, X-ray photoelectron spectroscopy; AP-Fe-NDC, amorphous-phase iron-naphthalenedicarboxylic acid; C-Fe-NDC, crystalline-phase iron-naphthalenedicarboxylic acid; TOF, turnover frequency; RRDE, rotary ring-disk electrode; OER, oxygen evolution reaction.

(ICP) measurement data are given in Table S2, which further proves that AP-Fe-NDC has more active sites.

Moreover, under the influence of eliminating the ECSA, the intrinsic activity of the catalysts was studied, and the LSV curves and Tafel graphs normalized by the C_{dl} value were also provided. After ECSA standardization, AP-Fe-NDC still possesses the smallest overpotential (Fig. S8a) and the lowest Tafel slope (Fig. S8b). The aforementioned result indicated that AP-Fe-NDC displayed better performance than C-Fe-NDC, which is attributed to the AP-Fe-NDC catalyst having a better intrinsic activity than C-Fe-NDC owing to its defect-rich structure. To further verify the inherent activity of the catalyst, the turnover frequency (TOF) was estimated (see the specific calculation details in SI). As illustrated in Fig. 4c, assuming that all materials on the modified electrode surface have catalytic activity for OER, the TOF values of AP-Fe-NDC, C-Fe-NDC, and IrO_2 are 0.483 s^{-1}, 0.0518 s^{-1}, and 0.009 s^{-1}, respectively. For the AP-Fe-NDC catalyst, the TOF values under different voltages are calculated, which are consistent with the aforementioned conclusions.

The oxygen yield and faraday efficiency were also evaluated using the rotary ring-disk electrode test. As shown in Fig. 4d, the ring current is about 0.2524 μA, much lower than the disk current, proving that the HO^{2-} generation ($2e^-$ process) on the AP-Fe-NDC electrode is negligible, confirming that the water oxidation process is a standard $4e^-$ process: $4OH^- \rightarrow O_2 + 2H_2O + 4e^-$. Simultaneously, the calculated faraday efficiency further illustrates the absence of other side reactions. As shown in Fig. 4e, the loop current is 1.6 μA and the disk current is 9.2 μA. The faraday efficiency was calculated to be 94%, revealing high selectivity to water oxidation.

3. Conclusions

In conclusion, the AP-Fe-NDC complex was designed using a facile and economic solvent substitution method. The prepared crystals deal with different solvents, and the crystal structure changed to the amorphous phase, making the particle size smaller and exposing more active sites, thereby promoting conduction. Whether it is under high or low current density, AP-Fe-NDC exhibits superb OER performance compared with C-Fe-NDC. The in situ generated FeOOH is considered active material for catalyzing reactions. Meanwhile, the use of 1,4-NDC with good conductivity can obtain a catalyst with excellent conductivity, both of which resulted in a significant improvement in the catalytic performance of OER. This work not only provides a way to improve the catalytic activity of coordination polymers but also expanded the application in water electrolysis.

Credit author statement

Yuan Xu: Data curation, Writing - original draft; Muhammad Arif Khan: Methodology, Software; Zhe Chen: Visualization, Investigation, Software, Validation; Cong Chen: Visualization, Investigation, Software, Validation; Lei Zhang: Software, Validation; Daixin Ye: Supervision, Conceptualization, Writing-Reviewing and Editing; Kangning Zhao: Software, Validation; Hongbin Zhao: Supervision, Conceptualization, Writing-Reviewing and Editing; Xueliang Andy Sun: Methodology, Software, Writing-Reviewing and Editing; Jiujun Zhang: Methodology, Software, Writing-Reviewing and Editing

Declaration of competing interest

The authors declare that they have no known competing financial interests or personal relationships that could have appeared to influence the work reported in this paper.

Acknowledgments

The authors gratefully acknowledge financial support from the National Key Research and Development Program of China (2017YFB0102900).

Appendix A. Supplementary data

Supplementary data to this article can be found online at https://doi.org/10.1016/j.mtener.2020.100564.

References

[1] J.J. Duan, S. Chen, C. Zhao, Ultrathin metal-organic framework array for efficient electrocatalytic water splitting, Nat. Commun. 8 (2017) 15341, https://doi.org/10.1038/ncomms15341.
[2] J.T. Li, W.Z. Huang, M.M. Wang, S.B. Xi, J.S. Meng, K.N. Zhao, J. Jin, W.W. Xu, Z.Y. Wang, X. Liu, Q. Chen, L.H. Xu, X.B. Liao, Y.L. Jiang, K.A. Owusu, B.L. Jiang, C.X. Chen, D.N. Fan, L. Zhou, L.Q. Mai, Low-crystalline bimetallic metal-organic framework electrocatalysts with rich active sites for oxygen evolution, ACS Energy Lett 4 (2018) 285–292, https://doi.org/10.1021/acsenergylett.8b02345.
[3] Q.Z. Qian, Y.P. Li, Y. Liu, L. Yu, G.Q. Zhang, Ambient fast synthesis and active sites deciphering of hierarchical foam-like trimetal-organic framework nanostructures as a platform for highly efficient oxygen evolution electrocatalysis, Adv. Mater. 31 (2019) 1901139, https://doi.org/10.1002/adma.201901139.
[4] M. Liu, L.J. Kong, X.M. Wang, J. He, X.H. Bu, Engineering bimetal synergistic electrocatalysts based on metal-organic frameworks for efficient oxygen evolution, Small 15 (2019) 1903410, https://doi.org/10.1002/smll.201903410.
[5] D.S. Raja, X.F. Chuah, S.Y. Lu, In situ grown bimetallic MOF-based composite as highly efficient bifunctional electrocatalyst for overall water splitting with ultrastability at high current densities, Adv. Energy Mater. 8 (2018) 23, https://doi.org/10.1002/aenm.201801065.
[6] S.L. Zhao, D.W. Wang, R. Amal, L.M. Dai, Carbon-based metal-free catalysts for key reactions involved in energy conversion and storage, Adv. Mater. 31 (2019) 1801526, https://doi.org/10.1002/adma.201801526.
[7] W.L. Li, F.S. Li, H. Yang, X.J. Wu, P.L. Zhang, Y. Shan, L.C. Sun, A bio-inspired coordination polymer as outstanding water oxidation catalyst via second coordination sphere engineering, Nat. Commun. 10 (2019) 5074, https://doi.org/10.1038/s41467-019-13052-1.
[8] K. Rui, G.Q. Zhao, Y.P. Chen, Y. Lin, Q. Zhou, J.Y. Chen, J.X. Zhu, W.P. Sun, W. Huang, S.X. Dou, Hybrid 2D dual-metal–organic frameworks for enhanced water oxidation catalysis, Adv. Funct. Mater. 28 (2018) 1801554, https://doi.org/10.1002/adfm.201801554.
[9] L.Z. Zhuang, L. Ge, H.L. Liu, Z.R. Jiang, Y. Jia, Z.H. Li, D.J. Yang, R.K. Hocking, M.R. Li, L.Z. Zhang, X. Wang, X.D. Yao, Z.H. Zhu, A surfactant-free and scalable general strategy for synthesizing ultrathin 2-dimensional metal-organic framework nanosheets, Angew. Chem. Int. Ed. 58 (2019) 13565–13572, https://doi.org/10.1002/ange.201907600.
[10] P.P. Su, S.S. Ma, W.J. Huang, Y. Boyjoo, S.Y. Bai, J. Liu, Ca^{2+} doped ultrathin cobalt hydroxyloxides from coordination polymers as efficient electrocatalysts for water oxidations, J. Mater. Chem. A. 7 (2019) 19415–19422, https://doi.org/10.1039/C9TA05882F.
[11] W.R. Cheng, X. Zhao, H. Su, F.M. Tang, W. Che, H. Zhang, Q.H. Liu, Lattice-strained metal–organic-framework arrays for bifunctional oxygen electrocatalysis, Nat. Energy. 4 (2019) 115–122, https://doi.org/10.1038/s41560-018-0308-8.
[12] Z.Q. Xue, K. Liu, Q.L. Liu, Y.L. Li, M.R. Li, C.Y. Su, N. Ogiwara, H. Kobayashi, H. Kitagawa, M. Liu, G.Q. Li, Missing-linker metal-organic frameworks for oxygen evolution reaction, Nat. Commun. 10 (2019) 1–8, https://doi.org/10.1038/s41467-019-13051-2.
[13] S.L. Zhao, H.J. Yin, L. Du, L. He, K. Zhao, L. Chang, G.P. Yin, H.J. Zhao, S.Q. Liu, Z.Y. Tang, Carbonized nanoscale metal-organic frameworks as high performance electrocatalyst for oxygen reduction reaction, ACS Nano 8 (2014) 12660–12668, https://doi.org/10.1021/nn505582e.
[14] S.L. Zhao, Y. Wang, J.C. Dong, C.T. He, H.J. Yin, P.F. An, K. Zhao, X.F. Zhang, C. Gao, L.J. Zhang, J.W. Lv, J.X. Wang, J.Q. Zhang, A.M. Khattak, N.A. Khan, Z.X. Wei, J. Zhang, S.Q. Liu, H.J. Zhao, Z.Y. Tang, Ultrathin metal–organic framework nanosheets for electrocatalytic oxygen evolution, Nature Energy 1 (2016) 16184, https://doi.org/10.1038/nenergy.2016.184.
[15] C. Li, Y.T. Gao, X.F. Xia, J.W. Zhu, X. Wang, Y.S. Fu, Hierarchically structured two-dimensional bimetallic CoNi-hexaaminobenzene coordination polymers derived from $Co(OH)_2$ for enhanced oxygen evolution catalysis, Small 16 (2020) 1907043, https://doi.org/10.1002/smll.201907043.
[16] F.L. Li, P. Wang, X.Q. Huang, D.J. Young, H.F. Wang, P. Braunstein, J.P. Lang, Large-scale, bottom-up synthesis of binary metal-organic framework nanosheets for efficient water oxidation, Angew. Chem. Int. Ed. 131 (2019) 7125–7130, https://doi.org/10.1002/anie.201902588.
[17] L. Yang, C. Qin, B.Q. Song, X. Li, C.G. Wang, Z.M. Su, Syntheses, structures, magnetic and luminescence properties of a series of coordination polymers

constructed from 1,4-naphthalenedicarboxylate and N-donor ligands, CrystEngComm 17 (2015) 4517–4524, https://doi.org/10.1039/C5CE00539F.
[18] B.X. Zhang, J.L. Zhang, C.C. Liu, X.X. Sang, P. Li, X. Ma, T.B. Wu, B.X. Han, G.Y. Yang, Solvent determines the formation and properties of metal–organic frameworks, RSC Adv. 5 (2015) 37691–37696, https://doi.org/10.1039/C5RA02440D.
[19] U. Martinez, J.H. Dumont, E.F. Holby, K. Artyushkova, G.M. Purdy, A. Singh, N.H. Mack, P. Atanassov, D.A. Cullen, K.L. More, M. Chhowalla, P. Zelenay, A.M. Dattelbaum, A.D. Mohite, G. Gupta, Critical role of intercalated water for electrocatalytically active nitrogen-doped graphitic systems, Sci. adv. 2 (2016) 1501178, https://doi.org/10.1126/sciadv.1501178.
[20] Q. Sun, M. Liu, K.Y. Li, Y. Zuo, Y.T. Han, J.H. Wang, C.S. Song, G.L. Zhang, X.W. Guo, Facile synthesis of Fe-containing metal-organic frameworks as highly efficient catalysts for degradation of phenol at neutral pH and ambient temperature, CrystEngComm 17 (2015) 7160, https://doi.org/10.1039/C5CE01375E.
[21] A. Dhakshinamoorthy, M. Alvaro, H. Garcia, Aerobic oxidation of cycloalkenes catalyzed by iron metal organic framework containing N-hydroxyphthalimide, J. Catal. 289 (2012) 259–265, https://doi.org/10.1016/j.jcat.2012.02.015.
[22] K. Nakamoto, Infrared Spectra of Inorganic and Coordination Compounds, John Wiley & Sons, 1963, p. 217, https://doi.org/10.1002/0470027320.s4104.
[23] X.X. Zhang, Q. Liu, X.F. Shi, A.M. Asiri, X.P. Sun, An Fe-MOF nanosheet array with superior activity towards the alkaline oxygen evolution reaction, Inorg. Chem. Front. 5 (2018) 1405–1408, https://doi.org/10.1039/C8QI00163D.
[24] H. Dong, X. Zhang, X.C. Yan, Y.X. Wang, X.J. Sun, G.L. Zhang, Y.J. Feng, F.M. Zhang, Mixed-metal-cluster strategy for boosting electrocatalytic oxygen evolution reaction of robust metal-organic frameworks, ACS Appl. Mater. Interfaces 11 (2019) 45080–45086, https://doi.org/10.1021/acsami.9b14995.
[25] L.S. Yang, Y. Liu, J.B. Li, G.P. Du, One-pot hydrothermal synthesis of amorphous FeOOH on Ni foam for high performance supercapacitors, J. Alloys Compd. 763 (2018) 134–140, https://doi.org/10.1016/j.jallcom.2018.05.305.
[26] X.F. Li, D.D. Ma, C.S. Cao, R.Q. Zou, Q. Xu, X.T. Wu, Q.L. Zhu, Inlaying ultrathin bimetallic MOF nanosheets into 3D ordered macroporous hydroxide for superior electrocatalytic oxygen evolution, Small 15 (2019) 1902218, https://doi.org/10.1002/smll.201902218.
[27] C. Wang, R. Wang, Y. Peng, J. Chen, J. Li, Iron tungsten mixed composite as a robust oxygen evolution electrocatalyst, Chem. Commun. 55 (2019) 10944–10947, https://doi.org/10.1039/C9CC05287A.